Aberystwyth University

Discovery of a New Class of Coronal Structures in White Light Eclipse Images
Druckmüller, Miloslav; Habbal, Shadia Rifai; Morgan, Huw

DISCOVERY OF A NEW CLASS OF CORONAL STRUCTURES IN WHITE LIGHT ECLIPSE IMAGES

Miloslav Druckmüller[1], Shadia Rifai Habbal[2], and Huw Morgan[2,3]

[1] Faculty of Mechanical Engineering, Brno University of Technology, 616 69 Brno, Czech Republic
[2] Institute for Astronomy, University of Hawaii, 2680 Woodlawn Drive, Honolulu, HI 96822, USA; shadia@ifa.hawaii.edu
[3] Institute of Mathematics, Physics and Computer Science, Aberystwyth University, Ceredigion, Cymru SY23 3BZ, UK

ABSTRACT

White light images of the solar corona, taken during total solar eclipses, capture the complex dynamic relationship between the coronal plasma and the magnetic field. This relationship can be recorded on timescales of seconds to minutes, within a few solar radii above the solar surface. Rays, large-scale loops, and streamers, which are the brightest structures in these images, have shaped current models of the coronal magnetic field and solar wind flow. We show in this work how the application of novel image processing techniques to unique high-resolution white light eclipse images reveals the presence of a new class of structures, reminiscent of smoke rings, faint nested expanding loops, expanding bubbles, and twisted helical structures. These features are interpreted as snapshots of the dynamical evolution of instabilities developing at prominence–corona interfaces and propagating outward with the solar wind.

Key words: eclipses – instabilities – solar wind – Sun: corona – Sun: filaments, prominences

1. INTRODUCTION

The naked-eye impression of the corona during a total solar eclipse is that of rays expanding in all directions from the solar surface, out to several solar radii. First captured in drawings, and subsequently with photography in the late 1800s, these impressions defined what we currently call "coronal structures." The most prominent rays emanate from the polar regions; they are ubiquitous throughout most of the solar cycle, with the exception of maximum sunspot activity. Streamers, characterized by bulges at their base and tapering off to thin rays with radial distance, become the dominant component at maximum solar activity. To the eye, the extent of the white light emission from the corona seems to be much larger at solar minimum than at solar maximum. Prominences, distinguished by their pinkish hue, invariably stand out during totality, irrespective of the time within a sunspot cycle. They are often considered by many eclipse chasers to be the highlight of the event.

The white light emission observed during total solar eclipses is a consequence of the scattering of photospheric emission by free electrons in the corona. Hence, the structures captured in eclipse images are not only tracers of the distribution of coronal electron density, but are also directly associated with coronal magnetic fields and outline their direction. The radial span and shape of these structures thus laid the foundation for models of the coronal magnetic fields (e.g., Munro & Jackson 1977). With the continued absence of direct measurements of coronal magnetic fields, eclipse images continue to serve as drivers as well as verifications for steady-state models of the corona and solar wind (e.g., Wang et al. 2007; Ambrož et al. 2009; Rušin et al. 2010; Antiochos et al. 2012).

However, the coronal plasma is far from static. It has to respond to turbulent motions associated with magnetic flux emergence leading to reconnection on all scales across the solar surface, to the production of MHD waves and to disturbances on much larger scales, such as filament eruptions and coronal mass ejections (CMEs). Despite their short duration (ranging from seconds to a maximum theoretical time of 7.15 minutes), and their paucity (occurring once every one to two years),

eclipse observations are well suited for studies of coronal dynamic events. Indeed, historical records show that a CME, albeit not recognized as such at the time, was recorded in an eye-witness image by A. Secchi during the eclipse of 1860 July 18 observed from Torreblanca, Spain. More recent eclipse observations captured the aftermath of the passage of CMEs in the inner corona (Habbal et al. 2011), and the development of an active region (Pasachoff et al. 2006). Observations of a given eclipse from different observing sites, separated by minutes to several hours, can also lend clues to dynamic events on those timescales. For example, the brightening of a polar plume was documented during the 2006 March 29 total solar eclipse from observations at two sites separated by 30 minutes (Pasachoff et al. 2008).

We show in this work how eclipse observations, described in Section 2, continue to yield novel insights into structures defining the coronal plasma and magnetic field despite the proliferation of space-based white light coronagraph observations of the extended corona and extreme-ultraviolet (EUV) observations very close to the Sun. In particular, we highlight the ubiquitous presence of smoke or vortex rings, expanding bubbles, nested loops, and twisted helical structures, mostly hitherto unknown (Section 3). Some of these structures seem to have counterparts in recently reported EUV observations very close to the Sun, and in white light coronagraph images beyond $2\,R_{\odot}$. Others remain unique to eclipse images, at present, although their occurrence seems to be validated by model studies and plasma laboratory experiments (Section 4). We conjecture that these newly discovered features originate at every prominence–corona interface and that the eclipse images capture snapshots of the different evolutionary stages of the ensuing instabilities. We briefly discuss their implications for the evolution of the solar wind (Section 5).

2. ECLIPSE DATA AND IMAGE PROCESSING

The white light eclipse data shown in Figures 1–3 are from our most recent observations of 2010 July 11, 2009 July 22, and 2008 August 1, respectively. They coincide with the beginning (2008) and the rising phase of solar activity cycle 24. The spatial

resolution in these images is 2″–3″. (See Habbal et al. 2010, 2011; Pasachoff et al. 2009, for more technical details regarding the acquisition of these data.) In addition, an example from the 2001 June 21 eclipse (Figure 4) taken from Angola at the peak of magnetic activity cycle 23, was selected for two reasons. (1) To show that the new class of structures, which will be described next, is ubiquitous in the corona even with observations taken with film and subsequently digitized, and (2) to explore whether their appearance has any solar cycle dependence.

The observations reported here were taken with Canon digital cameras (with the exception of Figure 4) with different focal length lenses. Details of the optics are described in the corresponding captions of Figures 1–4. In Figures 1–3, the full field of view of the corona is shown at the top, and close-up details within the outlines of the rectangles are given below.

Typically during totality, a sequence of at least 10 or more exposures is needed to cover the dynamic range of the coronal white light emission out to a few solar $R_{\odot}$. The application of sub-pixel alignment of images taken with different exposure times, a technique recently developed by Druckmüller (2009), as well as the application of the recently developed image processing technique referred to as the Adaptive Circular High-pass Filter (ACHF; Druckmüller et al. 2006), enable the creation of a single composite image with a resolution of 2″–3″. In general, the total effective exposure time needed for each image ranges from 20 to 50 s. The resulting composites expose the solar atmosphere starting from the upper chromosphere out to a distance of several solar radii all around the Sun. The lower chromosphere, down to the photosphere, near the east and west limb (Figures 1–4) may be exposed as well because these parts of the corona are progressively visible during any total solar eclipse. Observing the lower chromosphere near the northern and southern solar limb is complicated because it is either necessary to observe from locations near the edge of the shadow band of totality or the shadow band itself must be very narrow. In the both cases, the total eclipse is very short, on the order of a few seconds in duration.

Application of the ACHF to white light eclipse images also enables the enhancement of high spatial frequencies by about a factor of 300, such that structures with contrast 10^3 times fainter than the global contrast in an image becomes visible. Furthermore, this technique has the marked advantage of capturing faint structures within the context of the background "quiescent" large-scale coronal structures. Typically, dynamic or time-varying events, such as CMEs, are much fainter than the quiescent structures. CMEs were originally discovered with the space-based coronagraph on Skylab in the early 1970s using a simple running difference technique (e.g., Gosling et al. 1974). Such an approach is straightforward when a time sequence of observations spanning several hours is available. Recently, alternative techniques have been developed to expose faint dynamic structures, whereby a background, or quiescent corona, is defined and subtracted from a time sequence of images (e.g., Morgan et al. 2006, 2012). However, with such techniques, the dynamic structures are exposed while structures in the quiescent background corona are significantly reduced. Furthermore, such techniques are not applicable to eclipse observations since they rely on the availability of observations with extended time sequences. We demonstrate in what follows how the faint structures captured in eclipse images with the application of the ACHF are snapshots of non-stationary events, some of which were hitherto unknown.

3. A NEW CLASS OF CORONAL STRUCTURES

In the examples of the ACHF processed white light images shown in Figures 1–3, the corona is invariably dominated by ray-like structures. The most streamlined ones fill the polar regions. Away from the poles, these rays outline the shapes of streamers with arch-like structures defining their base. In Figure 4, taken at the peak of solar activity, the polar regions are indistinguishable from the rest of the corona, with streamers, loops, and rays distributed almost uniformly around the Sun. However, regardless of the time period within the solar activity cycle, a variety of features, clearly distinct from rays and streamers, with some significantly fainter, are invariably present in these eclipse images. In what follows, an attempt is made to classify them following some common characteristics.

3.1. Small-scale Loops and Vortex or Smoke-like Rings

We focus first on the plethora of small-scale structures that appear as a complex of small loops, typically 30″–40″ in height. These complexes are present in all images, within heliocentric distances of 1.1–1.2 $R_{\odot}$. Their details are best seen in the close-ups of Figures 1(A), 1(B), Figure 3, and almost everywhere around the limb in Figure 4.

Associated with, and/or embedded within these complexes are a few vortex or smoke-like ring structures, as seen in projection in the plane of the image. These appear most clearly in Figures 1 and 4. They are indicated by arrows numbered 4 and 5 in the close-ups of Figures 1(A) and 1(B). In Figure 4, the vortex rings (some of which are outlined by circles) seem to be present almost everywhere around the Sun. Unlike the features to be discussed next, neither small-scale loops nor vortex rings are necessarily faint in comparison with the dominant rays and streamers.

The feature labeled 3 in Figure 1 captures a mushroom-shaped plume. It is not clear if this feature has any connection to the vortex rings.

3.2. Nested Loops

Fainter systems of nested loops, discernible up to at least the first radius above the solar limb, are also ubiquitous in these eclipse images. They are present everywhere within the bulges of streamers, but are not limited to them. They appear to be self-similar, replicating themselves as a function of height with increasing size. To guide the eye, some examples are noted by arrows 1 and 6 in Figures 1(A) and 1(B). They abound in Figure 3 in the full field of view image everywhere above the prominences in the southeast, northwest and southwest, and in the details of Figure 3(A). The same applies to Figure 4, where they are present all around the Sun with different contrasts. Two examples are indicated by arrows.

3.3. Expanding Bubbles

Further away from the limb, a background of very faint and low contrast expanding bubbles, seemingly propagating away from the Sun, is clearly discernible and distinct from the large-scale nested loops. These are indicated by arrows 1, 2, and 3 in Figures 2(A) and 2(B). The most striking examples appear in Figure 3(A), with arrow 2 pointing to one example. The bubbles exhibit some structural coherence, and/or self-similarity, in a manner similar to that exhibited by the nested loops. They seem to form a faint background, filling a significant fraction of the corona, over at least a distance range of 1 $R_{\odot}$, especially at the
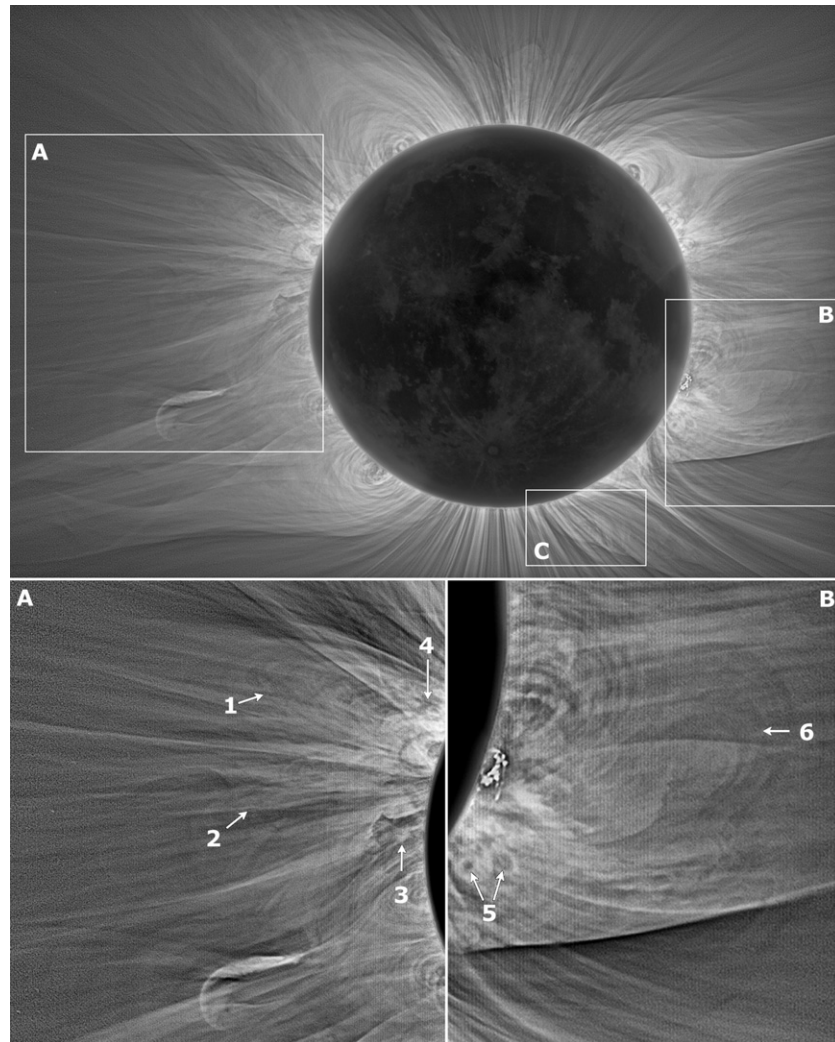
Figure 1. Top: white light eclipse image of 2010 July 11 taken from Tatakoto Atoll in French Polynesia, by Miloslav Druckmüller, Martin Dietzel, Shadia Habbal, and Vojtech Rušin. This image was produced from 61 images taken with a Canon EOS 5D digital camera and an 8/1624 mm Ritchey–Chrétien telescope. Details within the white rectangles labeled A and B are shown below. Arrows 1 and 6 point to concentric loops, 2 to screw-type helical structures, 3 to a mushroom-shaped plume, and 4 and 5 to vortex rings. Box C outlines the presence of a helical twisted structure at the boundary of the south polar coronal hole.

minimum of solar activity, such as in 2009 (Figure 2) and 2008 (Figure 3).

3.4. Twisted Helical Structures and Turbulence-like Structures

On a somewhat larger scale, we note the presence of twisted helical structures spanning a distance range of at least 0.5–1 $R_\odot$. The most prominent examples are present all around arrow 2 in Figure 1(A). An example is also visible in Figure 2, indicated by arrow 4. Note that these two examples are visually different, most likely representing the same type of structure viewed from different perspectives.

There is also a preponderance of turbulence-like structures in the eclipse images. One example is indicated by arrow 1 in Figure 3, and another is within the rectangle of Figure 4. Another example which could be equally interpreted as a twisted helical structure as well as a propagating turbulent structure appears at the west boundary of the south polar coronal hole, enclosed within the rectangle labeled C in Figure 1.

3.5. Impact of the Solar Cycle

As noted earlier, the choice of eclipse observations included a comparison of the impact of solar cycle effects. The differ-

ences, if any, should appear between the examples shown in Figures 1–4. As noted earlier, Figures 1–3 were acquired at the beginning of the rise of activity cycle 24. Figure 4 was taken at the peak of activity cycle 23. It is clear that the preponderance of vortex rings was largest in 2001, when solar activity was the highest compared to the 2008–2010 sequence of observations. The corona was the faintest in 2009. No vortex rings were detected then, but the field of view was rife with faint nested loops and expanding bubbles.

4. DYNAMIC CORONAL STRUCTURES AND THEIR ORIGIN

The examples presented above document the ubiquitous presence of a class of structures clearly distinct from the background corona of rays and streamers. Close to the Sun, the small-scale nested loops, as well as the vortex rings, typically 20″–30″ in height, are comparable in brightness to the background corona in these images. On the other hand, the large-scale nested loops, bubbles, and twisted helical structures are about two to three orders of magnitude fainter, and extend out to several solar radii above the limb. The impression one gets from the latter features is that of dynamic events, expanding
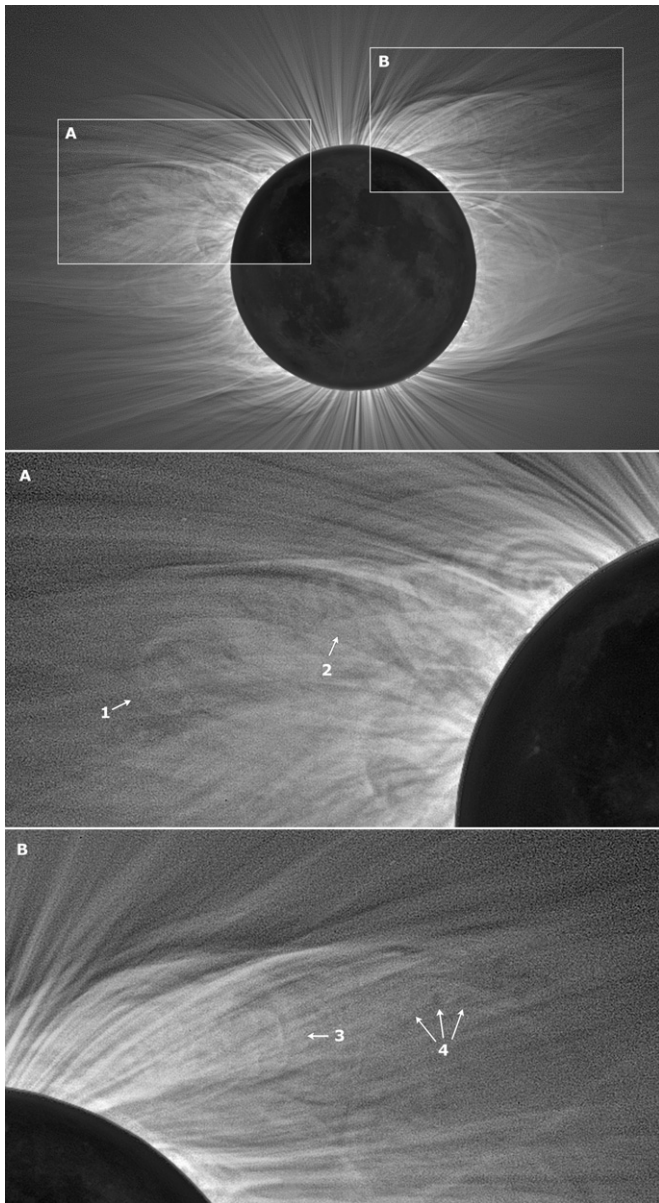
Figure 2. Top: white light eclipse image from 2009 July 22 eclipse taken from Enewetak Atoll in the Marshall Islands, by Miloslav Druckmüller, Peter Aniol, Martin Dietzel, Vojtech Rušin, L'ubomír Kl'ocok, and Karel Martišek. This image was composed from 31 exposures taken with a Canon EOS 5D digital camera and an 11/965 mm lens. Close-up details within panels A and B are shown below, where arrows 1, 2, and 3 point to faint expanding bubbles. Arrows 4 point to faint twisted helical structures akin to propagating vortices.

Figure 3. Top: white light eclipse image from 2008 August 1 observed from Mongolia, by Miloslav Druckmüller, Martin Dietzel, Peter Aniol, and Vojtech Rušin. The coronal image was produced from 25 images taken with a Canon EOS 1Ds Mark III digital camera and an 11/1250 mm lens. In the close-up details of rectangle A, Arrows 1 and 2 point to expanding twisted helical structures and screw-type expanding bubbles. Turbulence-like structures are also observed around Arrow 1.

away from the solar surface. Undoubtedly, if these features are dynamic, then they must be related to known dynamic structures at the Sun. Prominences are the prime candidate: when observed in projection off the limb, they exhibit continuous rising, falling and twisting motions, with counter-flows running along their complex magnetic structures. Their most violent eruptions lead to CMEs.

We argue in what follows that the class of structures detected in the white light eclipse images are inherently associated with the dynamic behavior of prominences. They are a natural consequence of the prominence–corona interface between a cool and dense plasma embedded in a hot and tenuous background, with shear flows developing between them. The inevitable consequence for this interface is the development of instabilities,
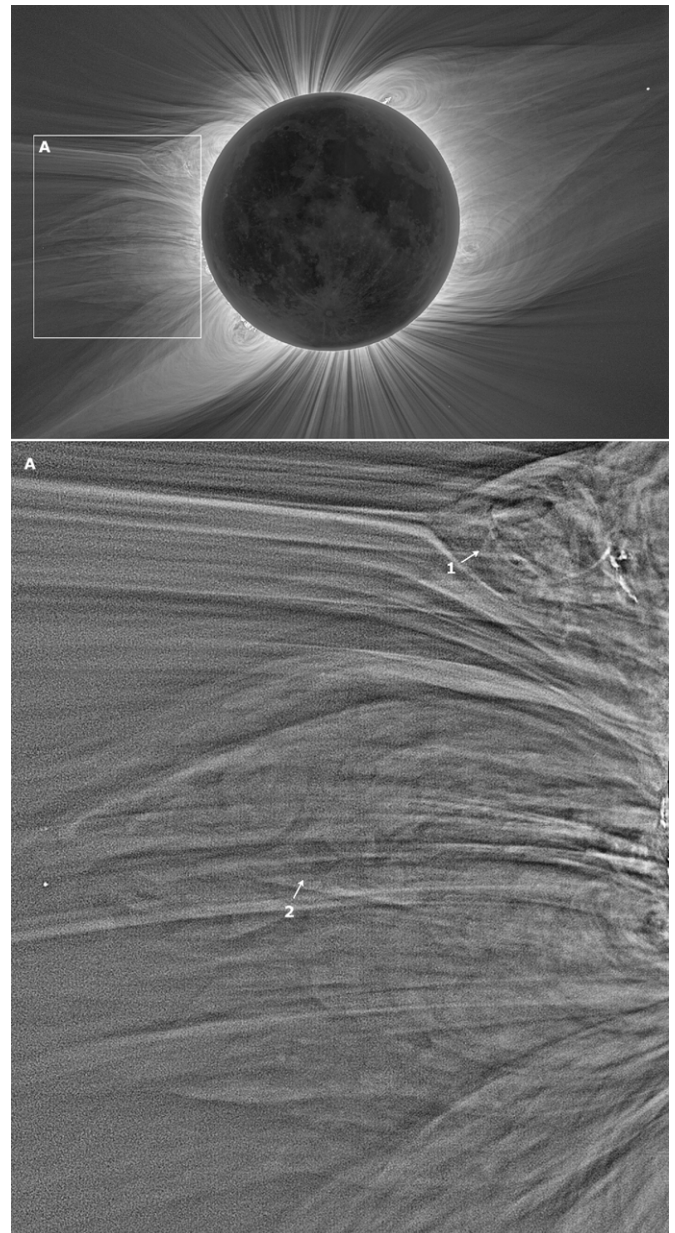
vortices, and turbulence in its immediate vicinity. The Earth's magnetopause is a prime example of a similar interface where the development of a Kelvin–Helmholtz (KH) instability and the formation of vortices have been observed (see, e.g., Hasegawa et al. 2004).

4.1. Nested Small-scale and Expanding Faint Loops

Prominences are known to straddle regions of opposite magnetic field polarities. While a prominence lies above a polarity inversion line, the opposite polarity magnetic fields on either side are bound to connect and form loops, starting very low down in the corona, and increasing in size with radial distance. Both polar crown and active region prominences are observed
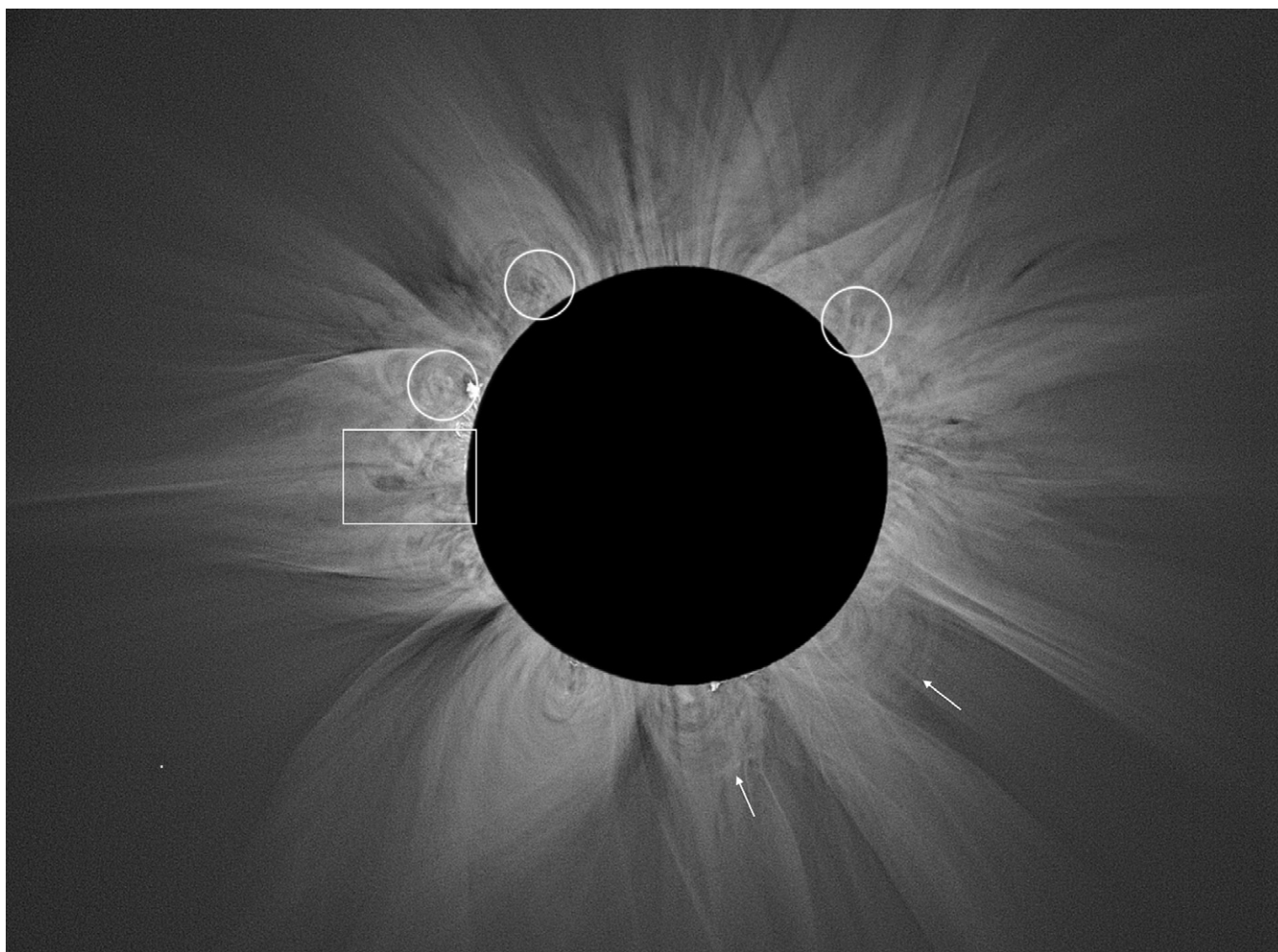
Figure 4. White light eclipse image from 2001 June 21 observed from Angola by members of the Úpice observatory, using a siderostat with an off-axis configuration and a 19/1875 mm lens. The image was composed from eight exposures taken on Kodak Echtachrome 100 S professional slide film, which was then scanned. The scanned image was processed by M. Druckmüller. The circles highlight examples of vortex rings. There is also an abundance of nested loops all around the Sun, the most prominent groups noted by arrows at the south pole and in the southwest. The rectangle highlights a region of turbulence.

off the limb in eclipse images, and the small-scale bright loops invariably straddle them. However, there is no reason why these loops should have a limiting size since magnetic field lines have no limiting sizes either. We propose that the faint expanding loops detected in the eclipse images are snapshots of the slow rise of the bright nested loops close to the Sun, overlying quiescent prominences. Whatever magnetic forces are driving the motions observed in prominences must have an impact on the seemingly more streamlined loops.

The most relevant data for comparison are the Large Angle and Spectrometric Coronagraph Experiment (LASCO)/C2 observations. Recently, Morgan (2013) and Morgan et al. (2013) applied the quiescent background separation technique (Morgan et al. 2012) to the LASCO/C2 data, and found evidence for the presence of faint rising nested loops above active regions, beyond the typical field of view of the Advanced Imaging Assembly on the *Solar Dynamic Observatory* (AIA/*SDO*) EUV imager. These rising loops could readily be a subset of the plethora of nested loops detected in the white light eclipse images, starting from the smallest and brightest ones very close to the solar surface, to the fainter ones detected almost out to $1\,R_\odot$. In the eclipse images these loops are not limited to active regions, as they appear almost everywhere above prominences except in the polar regions when the Sun is not at

the peak of solar activity. It is therefore plausible that the LASCO/C2 nested loops also straddled prominences within active regions. The novel contribution of the eclipse images, in comparison with the LASCO/C2 observations, is to capture the source of the faint loops in the inner corona and their expansion within the context of the large-scale structures of the background corona.

4.2. Vortex Rings, Twisted Helical Structures, and Expanding Bubbles: Evidence of Plasma Instabilities?

The detection of vortex-like rings, mushroom-shaped plumes, expanding bubbles, and twisted helical structures in eclipse white light images should not come as a total surprise. After all, the prominence–corona interface provides an ideal medium for the development of KH and Rayleigh–Taylor (RT) plasma instabilities (e.g., Ryutova et al. 2010; Soler et al. 2012).

Curiously, only two observations of vortex rings in the inner corona have been documented, and both were associated with prominences. These date back to the early 1970s, several decades before the advent of space-based observations. One was associated with a flaring activity (for comparison with the eclipse observations, see Figures 1 and 4 in Hagen & Neidig 1970), very likely to be triggered by a prominence eruption, and

the other directly with a prominence eruption (Kawaguchi et al. 1972). No other observations have been reported since then.

Using *Hinode* observations, Berger et al. (2010), Berger (2012), and Ryutova et al. (2010) recently provided observational evidence for the presence of plasma instabilities within quiescent prominences, as a consequence of turbulent upflows associated with bubbles rising from the chromosphere beneath the lower boundary of a prominence. These bubbles seemed to infiltrate the prominence assuming the shape of plumes characteristic of RT instabilities between the interface of two different density plasmas. According to these authors, this turbulent interface subsequently led to the formation of KH-generated vortices. A mushroom-shaped plume, associated with a prominence, was also reported by Ryutova et al. (2010; see their Figure 11) and Berger et al. (2010) and interpreted as such.

Foullon et al. (2011) recently reported on the formation of a KH instability and vortices at the boundary of a rising CME observed in the EUV with the AIA/*SDO* instrument. While no mention of a prominence eruption was made by these authors, the CME was very likely to have originated from a prominence eruption. The example encircled by box C in Figure 1 was also a result of the passage of a CME within the field of view prior to totality. This CME complex also produced the sharp wedge-shaped structure further to the north and reported in Habbal et al. (2011).

Amply documented and studied in fluids and laboratory plasmas, KH and RT instabilities are invariably associated with the presence of vortex rings (Jun et al. 1995; Lim 1997). Whether vortex rings trigger these instabilities, or are a consequence of them, is still not definitively established. The evolution of vortex rings into expanding bubbles and twisted helical structures as a consequence of a KH instability, has been visually captured in a wide range of laboratory experiments (Lim & Nickels 1995). On the other hand, numerical models of magnetized plasmas indicate that vortex rings are created from KH instabilities (e.g., Jun et al. 1995), as also documented by the magnetopause observations of Hasegawa et al. (2004). Numerical models also show that mushroom-shaped plumes (such as arrow 3 in Figure 1) arise as a consequence of RT instabilities (Hillier et al. 2012).

It is likely that the EUV-observed vortices, bubbles, and mushroom-shaped plumes continue to rise through the prominence and/or CME system to reach radial distances no longer detectable in the EUV and outside the field of view of the current EUV space-based imagers. Since eclipse images are snapshots of the instantaneous state of the coronal plasma, we can indeed expect to capture the different stages of the evolution of vortex rings, as illustrated in the examples described above. The fact that the vortex rings appear very close to the Sun, while the expanding bubbles and twisted helical structures are detected further away, lends additional supporting evidence for a natural connection between these structures, which most likely results from the evolution of instabilities at the prominence–corona interface.

5. DISCUSSION AND CONCLUSION

The observations presented here underline the main advantages of eclipse images in capturing snapshots of the coronal state, starting from the solar surface and spanning several solar radii outward. Tracking the dynamic evolution of small-scale structures and plasma instabilities originating in the inner corona, as they propagate outward, remains challenging. The

EUV observations from AIA/*SDO* have an unmatched temporal and spatial resolution. Yet, they remain limited to the first $0.25\,R_\odot$ above the surface due to the density square dependence of the emission. Unlike eclipse observations, the fate of dynamic structures as well as the appearance of dynamic events in the context of large-scale structures is excluded from EUV observations. On the other hand, the inner field of view of the best resolution space-based white light coronagraph at present, namely *Solar and Heliospheric Observatory*/LASCO C2, is blind to the first radius above the limb. Because of the light diffraction on the occulter it is impossible to build a coronagraph with an internal occulter that can provide images of the inner corona with the quality comparable to that attained with total solar eclipses. Hence, the origin of large-scale quiescent and dynamic structures at the Sun will remain inherently missing from the coronagraphic observations.

The unique observing conditions afforded by total solar eclipses, and the advent of state-of-the art image processing techniques, such as the ACHF, have made it possible to detect and capture the evolution of a plethora of structures within the context of the background corona. The absence of coronal observations, covering the distance range of eclipse images, are the most likely reasons why their preponderance has not previously been reported before. The presence of the new class of structures reported here cannot go unnoticed. They most likely reflect the different manifestations of plasma instabilities that inevitably arise in a complex magnetized plasma such as the corona.

We conjecture that the state of the corona reflects a spectrum of dynamic events. Some of these events are in the form of prominence eruptions and CMEs. Others are more subtle and form a continuum of faint structures such as the ones reported here. In fact, the structure of the corona, even on large scales in some cases, cannot be interpreted in terms of static structures. Indeed, static models of the corona (such as PFSS extrapolations) are limited in their scope due to the intrinsic dynamic nature of coronal structures.

It is plausible that this spectrum of dynamic events is the inevitable consequence of the development of instabilities at the prominence–corona interfaces that abound in the corona. Some supporting evidence can be gleaned from the observed difference between the structures captured at solar maximum in comparison to solar minimum and the rising phase of solar activity. At solar minimum (2009, Figure 2), there was an abundance of faint rising bubbles and nested loops. No vortices were captured at that time. At the other extreme, at solar maximum (2001, Figure 4), there was a plethora of vortices and turbulence-like structures around the Sun. Polar-crown filaments, which essentially define the boundaries of polar coronal holes at the Sun, and the magnetic polarity inversion there, are known to be relatively stable in comparison with active region prominences. Coronal structures are much simpler in the polar regions, hence prominence–corona interfaces there are expected to be more stable; the presence of the large-scale nested loops and bubbles is evidence for the extension of large-scale loops above polar crown filaments. In contrast, the complexity of coronal structures at solar maximum is such that prominence–corona interfaces, in particular within active regions, are bound to be prone to instabilities, hence the proliferation of vortex rings.

At present, the complexity of coronal structures, as presented in the examples given here, does not factor in MHD models of the corona. An example of the importance of this complexity

can be inferred from Figure 5 of Riley et al. (2012). These authors show how the complexity of the current sheet in their simulation increases significantly with the spatial resolution of their computational grid, in particular the appearance of spiraling structures near the equator, and the complicated boundary between the polar coronal holes and mid-latitudes. While their model is not directly related to vortex rings or the small-scale features we are reporting here, their example illustrates that simulations cannot at the moment account for the complexity at small scales, which are ubiquitous in the corona. Hence, at present, much is lost in simulations when one is attempting to understand the role of small-scale structures.

We should also caution that white light coronal images, like all remote sensing imaging, show emission along an extended line of sight. Hence, the interpretation of fine- scale and faint structures cannot necessarily be considered unique. The complex appearance of the corona, particularly after the application of image processing which enhances smaller-scale and fainter features, can partly be attributed to the alignment of structures along the line of sight. For example, it would be difficult to distinguish a small flux rope viewed along the tube axis from a vortex ring. The only reliable way to discriminate between the two would be higher resolution and higher cadence white light observations of the lower corona than the ones presented here. At present, the different faint structures reported in these eclipse observations support the vortex ring interpretation and corresponding instabilities in favor of flux tubes.

As noted by M. Ryutova (2012, private communication), vortex rings have the interesting property whereby their energy increases as their radius expands with their propagation. Hence, their role in the solar wind flow warrants future exploration. Morgan (2013) also pointed out that the rising nested loops could be carrying material which eventually forms the slow solar wind. While studies of models of CMEs currently abound, it is timely to consider the impact of the much more prevalent prominence-corona dynamic interface on the solar wind flow.

We emphasize in closing that the main goal of this work is to unveil and report on the presence of coronal structures, which have not been observed in the past. We have provided one interpretation, namely, the occurrence of instabilities at the prominence–corona interface, starting with the formation of vortex rings. Its validation, or the validation of alternative interpretations, requires more data. Processing archived film eclipse images, which are one source that has not yet been tapped into, is planned for the future. There is no doubt that much modeling and theoretical work are needed as well to fully assess the impact of these new class of structures on our understanding of coronal dynamic structures and the solar wind.

REFERENCES

Ambrož, P., Druckmüller, M., Galal, A. A., & Hamid, R. H. 2009, SoPh, 258, 243

Antiochos, S. K., Linker, J. A., Lionello, R., et al. 2012, SSRv, 172, 169

Berger, T. 2012, in ASP Conf. Ser. 454, Hinode-3: The 3rd Hinode Science Meeting, ed. T. Sekii, T. Watanabe, & T. Sakurai (San Francisco, CA: ASP), 79

Berger, T., Slater, G., Hurlburt, N., et al. 2010, ApJ, 716, 1288

Druckmüller, M. 2009, ApJ, 706, 1605

Druckmüller, M., Rušin, V., & Minarovjech, M. 2006, CoSka, 36, 131

Foullon, C., Verwichte, E., Nakariakov, V. M., Nykyri, K., & Farrugia, C. J. 2011, ApJL, 729, L8

Gosling, J. T., Hildner, E., MacQueen, R. M., et al. 1974, JGR, 79, 4581

Habbal, S. R., Druckmüller, M., Morgan, H., et al. 2010, ApJ, 708, 1650

Habbal, S. R., Druckmller, M., Morgan, H., et al. 2011, ApJ, 734, 120

Hagen, J. P., & Neidig, D. F. 1970, ApJ, 161, 751

Hasegawa, H., Fujimoto, M., Phan, T.-D., et al. 2004, Natur, 430, 755

Hillier, A., Berger, T., Isobe, H., & Shibata, K. 2012, ApJ, 746, 120

Jun, B.-I., Norman, M. L., & Stone, J. M. 1995, ApJ, 453, 332

Kawaguchi, I., Oda, N., & Mizuno, S. 1972, SoPh, 22, 140

Lim, T. T. 1997, FlDyR, 21, 47

Lim, T. T., & Nickels, T. B. 1995, Vortex Rings, in Fluid Vortices, ed. S. I. Green (Dordrecht: Kluwer), See also other publications, and examples from T. T. Lim's website: http://serve.me.nus.edu.sg/limtt/#Video_Gallery

Morgan, H. 2013, MNRAS, 433, L74

Morgan, H., Byrne, J. P., & Habbal, S. R. 2012, ApJ, 752, 144

Morgan, H., Habbal, S. R., & Woo, R. 2006, SoPh, 236, 263

Morgan, H., Jeska, L., & Leonard, D. 2013, ApJS, 206, 19

Munro, R. H., & Jackson, B. V. 1977, ApJ, 213, 874

Pasachoff, J., Kimmel, S. B., Druckmüller, M., Ruin, V., & Saniga, M. 2006, SoPh, 238, 261

Pasachoff, J., Ruin, V., Druckmüller, M., et al. 2008, ApJ, 682, 638

Pasachoff, J. M., Rušin, V., Druckmüller, M., et al. 2009, ApJ, 702, 1297

Riley, P., Linker, J., Lionello, R., & Mikić, Z. 2012, JASTP, 8, 1

Rušin, V., Druckmüller, M., Aniol, P., et al. 2010, A&A, 513, 45

Ryutova, M., Berger, T., Frank, Z., Tarbell, T., & Title, A. 2010, SoPh, 267, 75

Soler, R., Díaz, A. J., Ballester, J. L., & Goossens, M. 2012, ApJ, 749, 163

Wang, Y.-M., Biersteker, J. B., Sheeley, N. R., Jr., et al. 2007, ApJ, 660, 882